High-resolution inverted x-ray photoelectron diffraction studies of Si(100)

1997 J. Phys.: Condens. Matter 9 1967

(http://iopscience.iop.org/0953-8984/9/9/011)

J. Phys.: Condens. Matter **9** (1997) 1967–1982. Printed in the UK PII: S0953-8984(97)79124-0

High-resolution inverted x-ray photoelectron diffraction studies of Si(100)

Stephen Evans

Electron Spectroscopy Laboratory, Institute of Earth Studies, University of Wales, Aberystwyth, Dyfed SY23 3DB, UK

Received 31 October 1996, in final form 16 December 1996

Abstract. An inversion of the x-ray photoelectron diffraction (XPD) experiment has been performed in which *incident* electrons are diffracted to reach different sites within a crystal with differing relative probabilities reflecting those for *escape* of photoelectrons from the same sites in the corresponding XPD experiment. The diffracted-electron flux arriving at each site was monitored by using a Si(Li) detector to measure the intensity of the characteristic x-ray emission following core ionization by the incident electrons. This new technique, termed 'inverted' x-ray photoelectron diffraction (iXPD), has been initially applied to Si(100) for rotation about ⟨110⟩, and the expected close parallels between XPD and iXPD data have been observed. Although the intensity of the Si Kα x-ray signal increased rapidly as the incident-beam energy was increased beyond the threshold value for core ionization, the extent of the angular anisotropy correspondingly decreased, and there was little advantage in terms of signal:noise ratio in the iXPD pattern in increasing the energy to more than 10–15 eV above the threshold. The reduction in anisotropy resulted from a progressive degradation of the directional integrity of the electron beam by inelastic energy-loss processes. The angular resolution in iXPD is governed by the incident-beam divergence, which can easily be as small as $\sim 1^\circ$, much less than the angular acceptance of typical electron energy analysers. High-resolution iXPD data taken $\sim$10 eV above the threshold showed up to 38% angular anisotropy, much more than for conventional XPD at $\sim 3^\circ$ angular resolution, while iXPD data taken as much as 15–30 eV above the threshold still revealed splittings of all of the principal forward-scattering maxima of $\sim 5^\circ$. Similar splittings have been reported for high-resolution XPD of other systems, but not for Si(100). Their origins are briefly discussed.

1. Introduction

There has in recent years been an increasing interest in the application of x-ray photoelectron diffraction (XPD) to the determination of surface and near-surface structures [1–3], with over 100 papers published in each of the last three years. However, despite the technological importance of silicon, relatively few papers on XPD in Si have hitherto appeared [4–14], and none of these offers high-resolution polar-angle data for the (100) face. Angular resolution in XPD is frequently limited in practice by the specification of the electron energy analyser: a novel approach to high-resolution analyser design has been described [15], but, as with the conventional approach, substantial reductions in signal intensity are inevitable as electrons are collected from a smaller solid angle. It has, however, been demonstrated that valuable fine structure is often revealed when high angular resolution ($\sim 1^\circ$ or less) is achieved [16, 12, 13].

This paper describes and evaluates a novel alternative route for obtaining essentially equivalent information, demonstrated in application to Si(100). Significantly higher angular

0953-8984/97/091967+16$19.50

resolution is attained than is offered by typical general-purpose electron energy analysers by reversing the direction of the diffracted electron beam. *Incident* electrons at any specified angle will be diffracted by the crystal, leading to differing probabilities of reaching crystallographically differentiated sites in just the same way that photoelectrons ejected from these sites in the conventional XPD experiment have differing probabilities of reaching the surface following emission in different directions. This 'reciprocity relation' was recognized in the XPD context both by the present author and by Egelhoff [17] some years ago, but until recently [18] there has been no direct experimental verification. In these experiments, the electron flux arriving at a specific elemental site is monitored by observing the characteristic x-ray emission from that site. For any specified element (and electron energy), a fixed fraction of the electrons arriving at the site will induce core ionization; and a fixed fraction of the resultant holes will decay to yield an x-ray photon, which may escape from the solid and be detected by a Si(Li) x-ray detector of the type routinely used in scanning electron microscopes. The angular resolution of the new experiment is governed by the divergence of the incident electron beam, which can easily be maintained at $\sim 1^\circ$ or less. However, although high resolution is readily attained, our experiments show, unfortunately, that high sensitivity (enabling data collection times to be short) is not at present practicable.

It is convenient to term this new procedure 'inverted' x-ray photoelectron diffraction (iXPD), to emphasize the expected close relationship with conventional XPD. However, it must be recognized that this is a distinctly different phenomenon from inverse photoemission, in which the energy of an incident electron beam is scanned, and the intensity variation of the emitted photon flux monitored to provide information on the structures of the unoccupied bands of the solid. When relatively high incident-electron energies ($\sim$1–5 keV) are employed, and photons are detected at one fixed energy, the resulting technique, termed bremsstrahlung isochromat spectroscopy (BIS), provides information only on the density of states in the solid [19]. For experiments using much lower incident energies, the term 'inverse photoemission spectroscopy' (IPES) is used; here $\boldsymbol{k}$-conservation allows detailed maps of the unoccupied bands to be elucidated [19, 20] and a strong angular dependence may be observed. In both experiments, however, the initial electronic excitation and the emission of the photon are linked: the core electrons are not excited. The present iXPD experiments involve instead a two-stage process: a core ionization event induced by a relatively high-energy electron in which $\boldsymbol{k}$-conservation is not important, so the only angular dependence should be that resulting from diffraction of the incident beam, followed by a subsequent (incoherent) event as the core hole decays with emission of a characteristic x-ray photon. The photons which form the signal in the BIS experiment thus merely comprise a small part of the background in iXPD.

The incident beam for iXPD should have an energy which is not greatly in excess of that required to ionize the relevant core shell of the target element(s), because as the beam scatters, with energy loss, its directional integrity becomes progressively degraded. Preliminary experiments on GaAs [18] have already shown that this energy restriction is an essential requirement, and the variation of the iXPD signal with incident-beam energy in the near-threshold region has therefore been investigated here in some detail.

2. Experimental procedure

An 0.56 mm thick wafer of (100)-oriented Si (99.999%, n-type with 55–280 ppm P; supplied by Advent Research Materials Ltd) was cleaved along $\langle 110 \rangle$ directions to provide a sample $\sim$8 mm $\times$ 30 mm, which was attached to the end of the probe using tantalum clips. The surface was cleaned by Ar-ion bombardment ($\sim$750 eV, 4 μA for at least 600 s)

and then annealed at red heat for several minutes by electron bombardment (5.5 keV, 3–5 mA) with the electrons incident on the back of the sample. Such surfaces yielded reproducible Si 2p XPD patterns which did not increase in intensity (i.e. they showed a constant extent of angular anisotropy) following increases in either bombardment or annealing time. Carbon, oxygen and nitrogen contamination levels were monitored by XPS: C and N contamination was negligible, but small amounts of oxygen were detected. No direct evidence was available to establish whether or not the surfaces exhibited the expected (2×1) reconstruction [5, 8, 14].

All of the data were collected using an AEI/Kratos ES200A electron spectrometer, to which a Kratos Auger electron gun (1 mm spot size) and an Oxford Instruments Pentafet ATW x-ray detector controlled by Link ISIS software had been added in the geometry shown in figure 1. The x-ray detector was mounted on a linear translator and could approach to within a few mm of the sample; when retracted a gate valve isolated the detector from the rest of the UHV system. After an initial outgassing period of several days, the residual pressure indicated by the system ion pump returned to its former value of $\sim 5 \times 10^{-10}$ mbar, although the pressure in the immediate region of the sample was probably somewhat higher. The window on the x-ray detector routinely withstands an atmosphere pressure differential, and has high transmission down to C Kα at 277 eV: the system is therefore capable of measurements on the light elements frequently encountered as adsorbates and of particular interest in the context of surface structure determination. The x-ray detector was advanced to within about 30 mm of the sample for iXPD data collection.

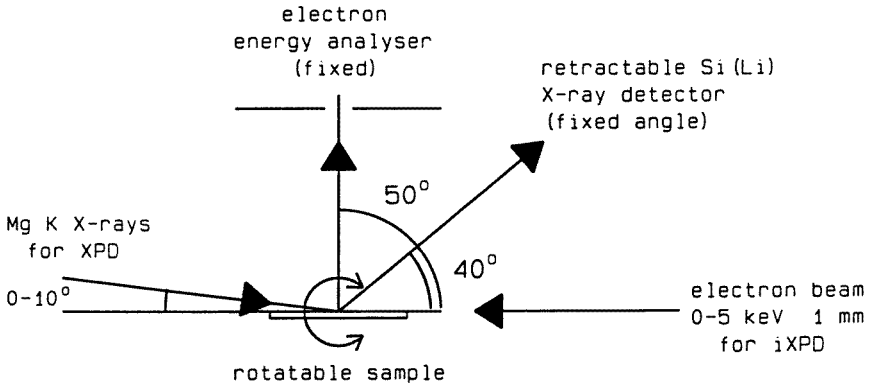

Figure 1. The experimental geometry for XPD and iXPD experiments on the same sample. The sample is shown horizontal (0° on the XPD take-off angle scale, 90° on the right-hand iXPD scales). Conventional XPD data collection associated with rotation through 90° anticlockwise yielded the right-hand side of the plot shown later in figure 3; a few additional data points could be obtained near 0° on the left-hand side by a clockwise rotation of up to ∼10°. The IXPD data collection corresponding to clockwise rotation from the position shown are associated with data points progressively from right to left in the iXPD plots in figures 4 and 5 (see later). Collection remains possible until the x-rays are detected at glancing exit (after probe rotation through 150° in all), with the electron incidence then at 50° to the surface normal: this is therefore the limiting value on the left-hand sides of figures 4 and 5.

XPD and 'inverted' XPD (iXPD) measurements were carried out on the same sample without breaking the vacuum. The angular resolution of the electron kinetic energy analyser for the XPS experiments was of the order of 3° in the plane parallel to the entrance slit, and somewhat greater in the plane at right angles to the slit [21]; the angular spread of

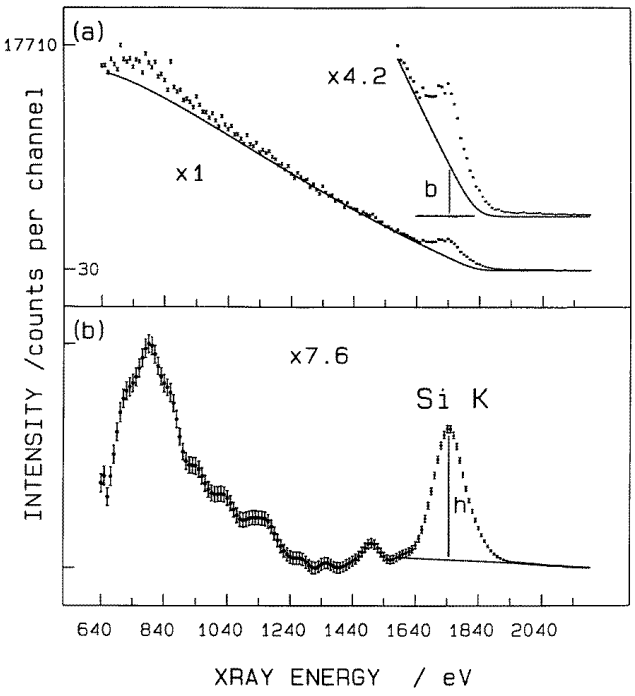

Figure 2. Data processing for a typical iXPD point. The incident-electron energy was 1849 eV, the incidence angle was 0°, and the data required 1200 s to collect (405 s live-time). The data are shown 'as collected' in (a), with the computed bremsstrahlung background overlaid; b indicates the background height at the Si Kα energy. The lower plot, (b), shows the data after smoothing and bremsstrahlung subtraction, with the net peak height labelled h. Subsequent iXPD diagrams track the behaviour of the ratio h/b. The data points are drawn with ± 1 standard deviation error bars on both plots; there are clearly non-random sources of channel-to-channel variation in (a) which are essentially averaged out by the smoothing process in (b).

the electron beam for the iXPD experiments was not precisely known, but with the beam focusing lens ~250 mm from the sample, it was expected to be ~1°.

Conventional XPD data (for comparison with the new iXPD results) were collected using Mg Kα radiation (with the x-ray detector fully retracted and isolated) for the Si 2p peak at 1151.8 eV, subtracting the background measured at 1154.8 eV kinetic energy. With source power of 300 W and counting times of 5 s, the statistical uncertainties (one standard deviation, σ) on the derived peak heights were ~0.5% throughout. However, because the instrument sensitivity is an (ill-characterized) function of angle, very dependent on precise sample location at the extremes of the angular range, it was necessary to normalize the data by reference to the similarly measured angular dependence of the signal from the same sample after Ar-ion bombardment (without annealing). Poor reproducibility in sample location near 0°, together with the fact that a median line had to be drawn through a small residual diffraction feature in the response function near normal exit, where the sampling depth is greatest, greatly increased the overall uncertainties in this region.

The incident-beam energy for the iXPD experiments was provided by a Brandenburg model 2507 power supply, adjusted to provide the precise energy required by using the XPS electron energy analyser to monitor the electron flux reflected from the sample surface. The

electron energy scale calibration was set to reproduce the known energy separation [22] between the Cu $2p_{3/2}$ and Au $4f_{7/2}$ XPS peaks from metallic specimens to within 0.08 eV, giving an expected precision of 0.01%, 0.2 eV in 2000 eV. The long-term stability of the electron beam energy was found to be ∼0.5 eV over several days, adequate for the present application. The 'effective spectrometer work function' (i.e. in practice, the zero offset of the indicated kinetic energy scale) was 2.2 eV, measured from the Si 2p kinetic energy (1151.8 eV) by taking the Si 2p binding energy as 99.6 eV [23]. The electron energies reported below are as recorded, and have not been corrected for this offset.

The incident-beam current was generally in the range 10–30 μA, typically 15 μA. The current was not regulated, and noticeable drift occurred. At these currents, the data collection rate was close to maximal, with the 'live-time' (the period during which pulses are being accepted by the discriminators) about one-third of the total data collection time ('real-time'). The discriminators were set for optimum resolution, to maximize the signal/background ratio, and in this mode the maximum count-rate was about 1.5 kcount s^{-1}. Adequate counting statistics could be achieved in 200–1200 s, depending on the beam energy: the actual data collection times used in each case are given in the figure captions.

Four series of iXPD measurements were made. Initially, the beam energy was varied over a wide range from below the threshold to 2500 eV, for a fixed sample orientation (usually normal electron incidence) and the Si Kα peak height/background (h/b) ratio evaluated. The first full iXPD data collection was then carried out ∼15 eV above the threshold, at 1854 eV. Two sets of data each covering the entire accessible angular range were collected at 2° angular increments, requiring $\sim 6 \times 10^4$ s (∼17 hours) in all to collect. Probe rotation and data collection were controlled manually throughout. The carbonaceous contamination which had developed was then recorded using XPS as well as x-ray emission. After automation of the probe rotation and data collection, the surface was reprepared, and a further two sets of data collected at 1869 eV. Finally, the surface was reprepared again, and a series of scans made at 1° angular increments across the structure centred at normal incidence with seven different electron energies in the range 1849–1884 eV, to examine the dependence of the anisotropy and fine structure on energy in the near-threshold region.

3. Data processing for iXPD

The raw spectra were smoothed by convolution with a Gaussian of 50 eV full width at half-maximum [24], and a continuum (bremsstrahlung) background estimated [25] as

$$f(E) = [k_1(E_0 - E)/E + k_2(E_0 - E)^2/E^2] \exp(-k_3/E^n)$$

subtracted from the spectrum. E_0 was set to the accurately known incident-beam energy, and the constants k_1 and k_2 were determined for each spectrum by fixing two background points and solving the resultant equations at fixed k_3 and n. The exponential term models the low-energy cut-off from the x-ray detector window, and has little effect near the threshold. To improve reproducibility, the fixed background points were each evaluated as the mean of nine channels; the centre points of each set lay near 850 and 1650 eV energy. Processing was automated (using FORTRAN77 on a 33 MHz 80486 personal computer) and once selected, the same values for k_3, n and the two background channel numbers were maintained throughout the data set. Any residual background was then removed (again, between fixed preset limits throughout) and net peak heights at the Si Kα maximum computed as the difference between the background line and the turning point of a quadratic fitted to the highest nine points in the net data. The stages in processing a typical spectrum are shown in figure 2.

Because the incident-beam current was not regulated, the peak height itself could not be used as a quantitative measure of the x-ray intensity. However, the height/background ratio is independent of the current used, and of the data collection time, and has proved to be an excellent measure of the peak intensity. (There is not expected to be any significant angular modulation in the intensity of the bremsstrahlung radiation excited concurrently by the electron beam.) The intensity of the computed continuum background, integrated over a 500 eV range, was found to show less apparently random variation than the value in a single channel at the peak maximum, so when evaluating the height/background ratio, the integrated background was used with an empirical conversion factor so that the quoted numerical values for height/background match the definition shown in figure 2. The actual values for the ratio will in any event be heavily dependent on the experimental details: the better the x-ray energy resolution, the higher the height/background ratio will become. In evaluating [26] the precisions of the height/background ratios, as represented in the diagrams, any contribution from the computed background was neglected.

It soon became apparent that a correction for the gradual build-up of adventitious carbonaceous contamination of the sample was required. Duplicate data points, recollected after a period of some hours of electron irradiation, showed markedly lower height/background ratios, while a carbon Kα x-ray peak had also developed. Variations in the low-energy background with angle prevented the direct automatic use of the C Kα peak intensity, so a procedure was adopted which used the total time of exposure to the electron beam, t, as an indicator of the amount of carbon present, since it was found that the rate of contamination in the absence of the electron beam (e.g. overnight) was negligible in comparison. Each Si Kα x-ray intensity was corrected by multiplying by $\exp(ft/[\lambda\cos\theta])$, where λ is the inelastic mean free path of the electrons, θ is the angle between the electron beam and the surface normal, and the factor f was evaluated empirically to minimize the overall scatter of the data. Estimating λ as $\sim$30 Å at $\sim$1850 eV [27], a contamination rate of $f = 9.33 \times 10^{-5}$ Å s^{-1} was found to yield the best results, corresponding to a total contamination layer thickness of 5.6 Å after collection of 100 data points requiring 600 s each (approximately correct for either full data set). XPS data were also collected before and after the iXPD data, and in both cases the increase in C 1s intensity indicated essentially the same rate of contamination (6.0 and 5.4 Å during iXPD data collection, respectively). Such a rate should not be taken to imply that introducing the Si(Li) detector seriously impairs the vacuum performance: if the sticking coefficient for beam-stimulated adsorption is unity, then the inferred partial pressure of the carbonaceous species would be in the low 10^{-11} mbar range. Other workers [14] using conventional XPD have found it desirable to reprepare their Si(100) surfaces after only two hours' exposure at $<2 \times 10^{-10}$ mbar.

The angular scales for the iXPD data were established by taking zero (normal incidence) as the centre of the band of emission in this region. The experimental geometry shown in figure 1 would lead to an expected difference of 90° between the zero points of the XPD and iXPD scales, but in practice a difference of only $\sim$87° was observed. This presumably arose as a consequence of deflection of the incident electron beam from the ideal sample centre-line and/or misalignment of the entrance slit of the electron energy analyser, together with the influence of stray magnetic fields.

4. Results and discussion

The conventional Si 2p XPD pattern is shown in figure 3. Previously reported data obtained at the same energy but at $<$7° resolution [5, 6], compared numerically in table 1, show essentially similar profiles, but with no resolved splitting of the structure near 0°, no obvious

Table 1. Angular features in XPD and iXPD for rotation of Si(100) about a ⟨110⟩ direction. (Unresolved shoulders are shown in parentheses.)

This work		Previously reported XPD data				
iXPD at 1849–1869 eV	XPD at 1152 eV	at 1337 eV [8][a]	at ∼1337 eV [11]	at ∼1152 eV [5][b]	at ∼600 eV [7][c]	Associated low-index direction[d]
0	(0)	0	0	0	n.r.	[001] (0°)
2.4 ± 0.2	3 ± 1				n.r.	
7.5 ± 1	(8 ± 1)				n.r.	
17.6 ± 1.5					(17)	
	19.4	19	19	19.1		[114] (19.4°)
22.3					25	[113] (25.2°)
32.0						
	33.4	32	31	34.4	37	[112] (35.2°)
35.9						
44.5	(∼40)	(39)	(40)		(41)	[445] (40.2°)
53.1	53.5	53.3	53	53.4	58	[111] (54.7°)
(58.5)	(57.2)					
68.7	68.5	68.9	66		(67)	[332] (64.7°)

[a]Measured from figure 7 of the cited paper.
[b]Measured from figure 2(b) of the cited paper.
[c]Measured from figure 4 of the cited paper.
[d]An excellent diagram showing these directions and angles in relation to a cross-section through the structure can be found in Puppin *et al* [7], figure 3. Kubler *et al* [5, 6] give similar but marginally less comprehensive diagrams.

asymmetry of the feature at 53°, and only an asymmetry rather than a clear shoulder near 40°. The weak feature at 67° was also not detected. However, Fraxedas *et al* [11], working at higher energy (Al Kα Si 2s, ∼1337 eV) but at similar angular resolution, reported a pattern virtually identical with figure 3, matching all the features closely except the incipient splitting of the 0° feature. The surfaces examined by both groups were known to exhibit the (2×1) reconstruction, from ultraviolet photoelectron spectroscopy and low-energy electron diffraction respectively. Tonner *et al* [8], also working at 1337 eV, again found a closely similar profile, recorded at an unspecified resolution, from a surface shown by photoelectron holography to exhibit the (2×1) reconstruction. However, these similarities are not sufficient to establish that the present surfaces also exhibit the (2×1) reconstruction. On flat surfaces, equal domains of (1×2) and (2×1) normally form [5], and experiments with vicinal surfaces where a single (2×1) domain predominates [5] revealed only relatively small differences between the XPD obtained in two azimuths distinguished by 90° rotation (compare figures 2(b) and 2(c) of reference [5]). These differences were felt [5] to lie within the experimental precision, so no firm conclusion should be drawn from the observation that the present data are markedly more similar to the former figure 2(b). The effects of any surface reconstruction are expected to be even smaller in the iXPD experiments in view of the relatively long electron inelastic mean free path, greater than in both the present and previous XPD studies.

At the much lower electron energy of 600 eV, for which data have been reported by Puppin *et al* [7], the structures are noticeably less well resolved, as one might expect [28], but the angular positions of the three main maxima observed are again in reasonable agreement.

The iXPD patterns corresponding to the XPD of figure 3, for the two electron energies for which full data sets were collected, are shown in figures 4 and 5, reproduced on the same abscissa scale for easy comparison. The two data sets collected at each energy are

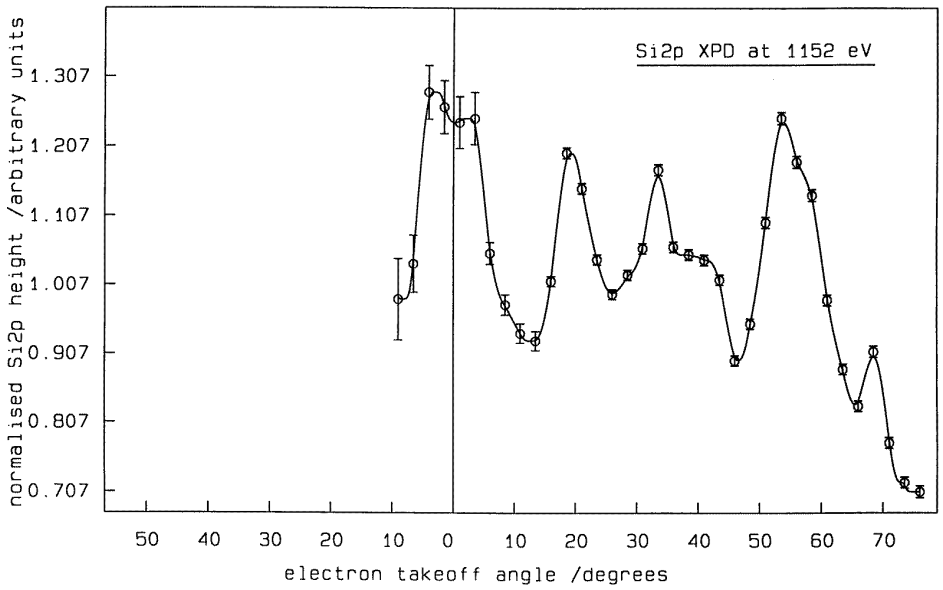

Figure 3. Si 2p XPD at 1151.8 eV photoelectron energy. The zero point on the angular scale corresponds to the sample in the position shown in figure 1, with the higher angles on the right attained by anticlockwise rotation. The error bars represent $\pm 1\ \sigma$; above 12°, these indicate the combined statistical uncertainties of the three counts involved, but near 0° uncertainties in the instrument response function and the reproducibility of the probe position are dominant—see the text.

shown superimposed in each case: after the correction for carbonaceous contamination, the duplicate set of points did not lie consistently above or below the initial sets, so there was no reason to distinguish them in the plots.

Superposition of figures 4 and 5 reveals excellent consistency as regards the existence and angular position of diffraction features, with somewhat poorer agreement as to their relative intensities. However, the only major discrepancy, in the relative intensity of the feature at 53°, which appears much more intense in figure 4, disappears if the two upper points defining that peak in figure 4, and which are several standard deviations above their duplicates, are discounted. Agreement is then generally excellent, with no evidence for a reduction in resolution accompanying the reduction in percentage anisotropy.

Crystal symmetry requires that the data show mirror planes at 0°, an expectation which is largely fulfilled. Angular positions on each side of the mirror plane correlate well, but there are some apparent changes in intensity. In particular, the feature between 30° and 40° seems more intense on the left-hand side of both figure 4 and figure 5. This may be due to crystal alignment errors: the cleaved edge of the crystal was set parallel to the probe axis by eye, and errors of up to a degree or so cannot be ruled out. Alternatively, there may be some unsuspected angular dependence in the intensity of the bremsstrahlung background used to normalize the peak height data, although this seems less likely: a mechanism for a weak dependence of photon flux on the angle between the incident electron and detected photon has however been described [29]. This uncertainty could be resolved in future work by studying amorphous silicon; even an ion-bombarded crystalline sample would probably be sufficiently disordered for this purpose. However, alignment errors remain the most likely

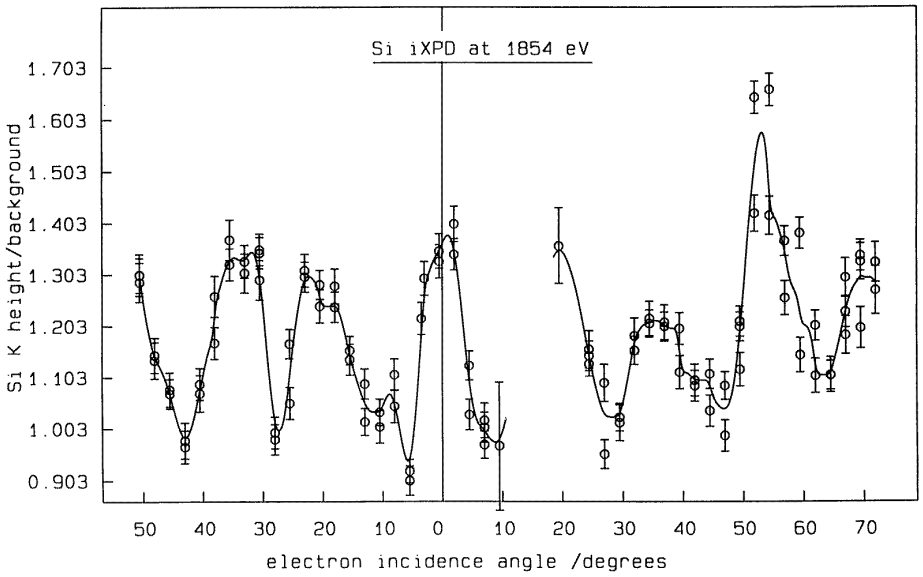

Figure 4. IXPD from Si(100) for rotation about a ⟨110⟩ direction, and incident-beam energy of 1854 eV. Two data sets are included, collected consecutively from the same surface. The data collection times were 200 s live-time per point, typically 600 s real-time; the error bars represent $\pm 1\ \sigma$.

explanation at present: effects of similar magnitude in conventional XPD for nominally symmetry-equivalent rotations have frequently been observed (e.g. [5]). Unfortunately, it is not possible to compare the relative intensities of the features at ∼10–20° off normal incidence on each side: it was found to be impossible to collect data for the right-hand sides of the diagrams in this range. At an electron incidence angle of 20°, reached by 70° clockwise rotation of the sample from the position shown in figure 1, the condition for specular reflection of the electron beam onto the Si(Li) detector was met, and near to this angle spurious zero-energy pulses saturated the detector.

If the statistical errors were the only significant source of uncertainty, duplicate iXPD data points should lie within 2 σ of each other, i.e. the uncertainty bars plotted should overlap, in 19 instances out of every 20. This standard is not quite maintained; where the ratio h/b is varying rapidly with angle, the estimated uncertainty in angle of ∼0.5° also becomes significant. Making qualitative allowance for this, the observed reproducibility is actually surprisingly close to statistical expectations considering the simplicity of the method used to correct for carbonaceous contamination: the correction factor amounts to as much as 1.35 at 50° by the end of 17 hours' data collection—causing an adjustment some 17 times greater than the statistical uncertainty. There will thus generally be a practical limitation on data quality (signal/noise ratio), determined at least in part by the rate of sample contamination *in vacuo*. It is of little value to collect data with very good counting statistics if at the same time uncertainties in the carbon contamination correction become far greater than the statistical uncertainties. The vacuum performance of any iXPD apparatus is thus of paramount importance.

The major features in the iXPD data obviously associated with near-neighbour directions correlate excellently with both the present and all previous XPD work, as shown in table

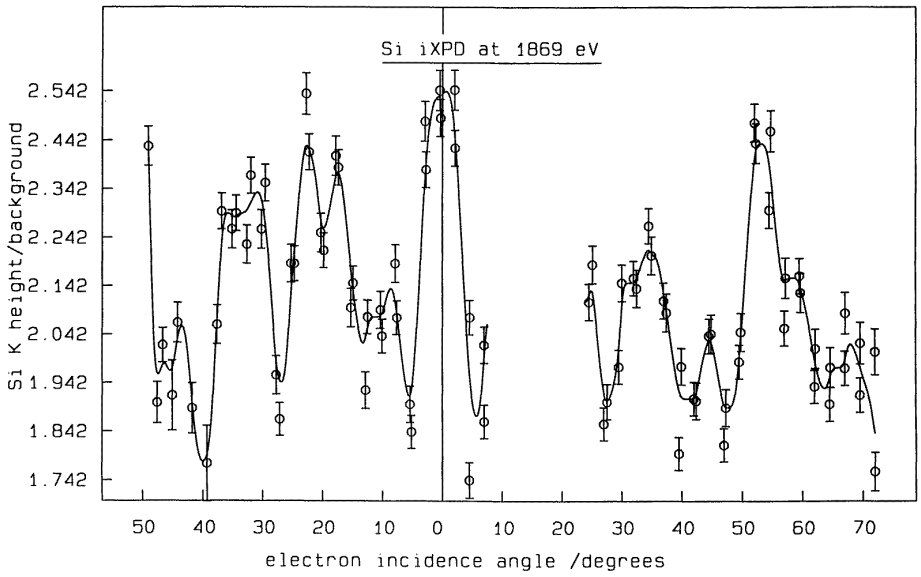

Figure 5. IXPD from Si(100) for rotation about a ⟨110⟩ direction, and incident-beam energy of 1869 eV. Two data sets are included, collected consecutively from the same surface. The data collection times were 600 s real-time per point, typically 200 s live-time; the error bars represent $\pm 1\ \sigma$.

1, although in the present high-resolution data the features centred at $\sim 19^\circ$ and $\sim 33^\circ$ are split. It is clear that the expectation that the iXPD experiment should yield closely similar data to those from XPD is entirely fulfilled. However, the agreement is not quantitative and there are some distinct differences. The feature near 19° appears, unexpectedly, to be rather less broad in the XPD plot, and the shoulder at $\sim 40^\circ$ in the XPD, confirmed by the closely similar profiles reported by Fraxedas *et al* [11] and Tonner *et al* [8], is much less prominent in the iXPD data. The most probable explanation for such differences is that they are secondary 'interference' [28] structures which vary with electron energy (wavelength): XPD data at 600 eV [7] again show significant detail differences while retaining the major maxima.

In addition, the feature at 0° is noticeably broader in the XPD data. The peak profile is rather flat topped, with an incipient splitting apparently masked by the data scatter in the iXPD plots in figures 4 and 5. More detailed scans of this feature in iXPD were therefore collected with 1° angular increments and for a range of incident energies from 10 to 45 eV above the threshold. These are shown in figure 6.

The lines drawn through the data points are scaled replicas of the mean data, showing that there is little, if any, broadening of the feature accompanying the reduction in anisotropy as the incident energy is increased. This shows that the recorded width of the feature is intrinsic, and it is also clear that the maximum intensity is not at 0°, as the simple forward-scattering model [30] would predict. The nominal scale (deduced from the data in figure 4, taken at 2° intervals) was seen to be slightly in error, and by summing the data for the four lowest energies and then reflecting the data about the true peak centre, a better representation of the peak profile was obtained, which is shown in figure 7.

These data confirm that this feature, associated with [001] forward scattering, is split

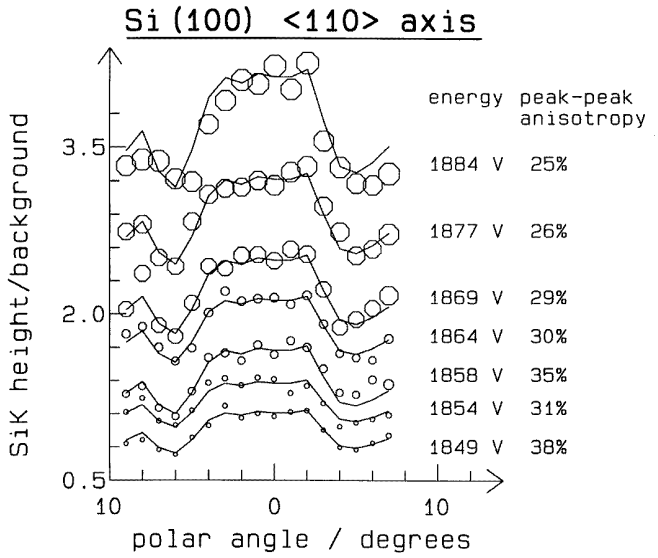

Figure 6. High-resolution iXPD scans of the feature for normal electron incidence taken at 1° angular increments, as a function of incident-electron energy. The data collection times (real-times per point) were 1200 s at 1849 and 1854 eV; 600 s at 1858 and 1864 eV; and 200 s for the remainder. The lines drawn through the data points are scaled replicas of the mean data. The peak–peak anisotropy is expressed as a percentage, defined as $200 \times (\max - \min)/(\max + \min)$.

into two, with (probably) a weaker central maximum as well. A similar triple-peaked profile has been reported [13] at high resolution (±1°) for the [100] forward-scattering XPD peak from Si(111) for the $[\bar{1}2\bar{1}]$ azimuth. (There is also a definite feature at 7–8°, confirming a weak peak seen in both of the data sets collected at 2° intervals.) The overall general shape of the [001] peak in both XPD and iXPD is strongly reminiscent of the typical Kikuchi-band profile expected [31] for XPD peaks associated with planes of high atomic density. The overall iXPD peak width (4.8° between maxima, FWHM 7–8°) is comparable with the (002) Bragg angle doubled (6°), as required by Kikuchi-band theory [31], and the greater splitting and additional width in the corresponding 1152 eV XPD data (6° between maxima, FWHM ∼11°) are simply explained as a consequence of the longer electron wavelength: twice the Bragg angle is here 7.6°. The enhanced-forward-scattering (EFS) model [30], which is now more frequently invoked to explain XPD features, would also predict that the peak should become sharper and more intense with increasing energy [28], but splittings of this nature are not qualitatively predicted by this approach.

The iXPD data for the whole angular range (figures 4 and 5, and table 1) also reveal that the other major features also show splittings of similar magnitudes, not observed previously at lower resolution. While the Kikuchi-band interpretation [31] would lead one to expect this, as discussed above, the EFS concept offers no qualitative guidance regarding the shape of the peaks. Splittings of this order are now frequently being detected with the advent of higher experimental resolution: for example, in MgO(001), where a splitting has recently been reported in the O 1s XPD (but not in the Mg KLL XPD) in the [001] direction [32, 33], which was not apparent at lower resolution [34], and in Si(111) for Si 2p at normal exit [13], where again no splitting was detected at lower resolution [9]. Single-scattering-cluster (SSC) calculations for Cu LMM Auger emission through a nickel (100) overlayer [28] show

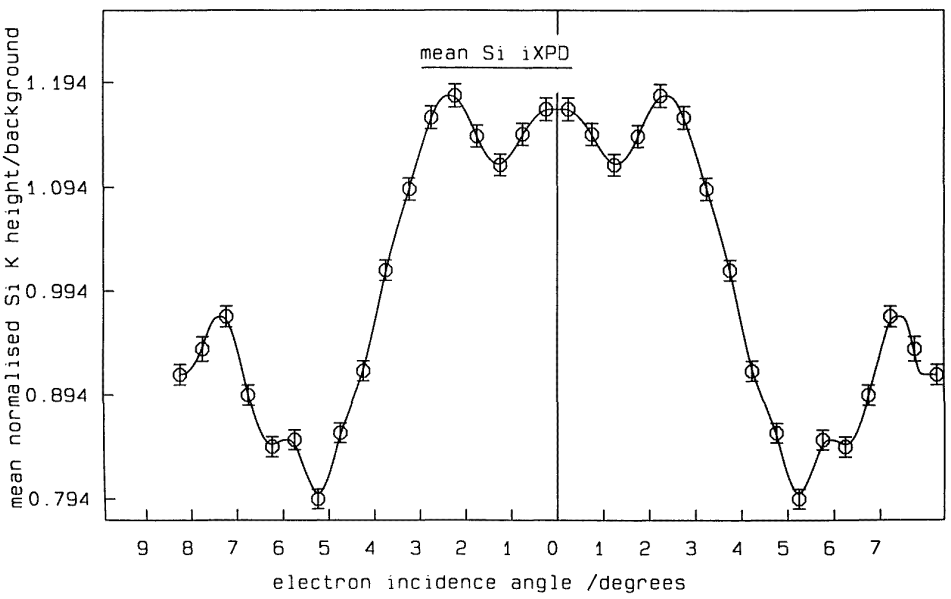

Figure 7. Data from figure 6 for the electron energies 1849 to 1864 eV, summed and reflected about the centre of the peak. At this high resolution, the nominal zero of the scale of figure 6 was seen to be very slightly in error (by $\sim 0.7^\circ$), so the reflection process, recognizing the symmetry inherent in the experiment, effectively doubles the number of points. Together with the improvement in the signal/noise ratio resulting from the summation, this enables one to recognize a triple structure in the main peak, and confirms the weak feature at $\sim 7^\circ$. Error bars again represent $\pm 1\ \sigma$.

a very similar effect at normal exit. It therefore seems that the Kikuchi-band-like profile is not universal, while the experimental splittings—where present—can be reproduced by SSC calculations [13, 32, 33] as effectively as by multiple-scattering theory [34]. In the case of MgO, the difference between the Mg and O diffraction profiles has been attributed to differences in the elastic scattering phase shifts between the two elements [32], but evidently such profiles can also arise in elemental solids [13]. The only calculations reported for the present rotation axis in Si(100) [11], also by the SSC method, do not show any splittings (and also fail to predict the pronounced shoulder at $\sim 40^\circ$). No mention was made [11] of any broadening function introduced to match theory to experiment at only 7° resolution, but it would appear to be possible: most calculated XPD patterns show much fine structure which is often not observed. Preliminary unpublished SSC calculations [35] show a profile for the peak at around 0° quite similar to that observed experimentally.

The lowest incident-beam energy at which the Si Kα peak was definitely detected ($h/b \sim 0.38$) was 1840 eV (1842.2 ± 0.7 eV referenced to the Fermi level), very close to the expected threshold of 1840.5 eV, the Si 1s binding energy (1839.3 eV [36]) plus the 1.2 eV band gap. Figure 8 shows the percentage anisotropy (defined as in figure 6) in the parameter h/b, and the parameter h/b itself, for the feature centred in the [001] direction, as functions of incident-beam energy. Since there is no significant difference between the iXPD profiles in figures 4 and 5, a similar variation would be expected for other directions of the incident beam.

The maximum attained anisotropy of $\sim 38\%$ at 1849 eV, ~ 10 eV above the threshold,

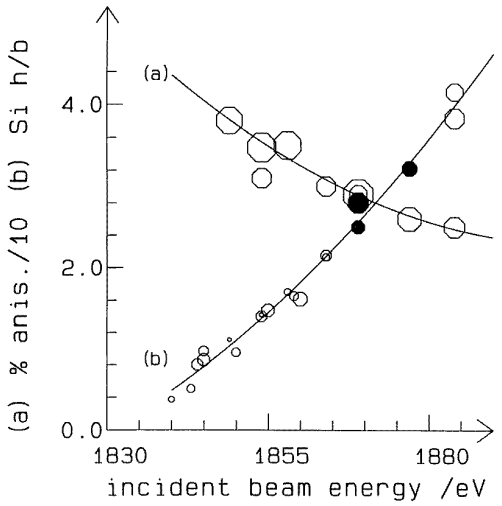

Figure 8. (a) The peak–peak anisotropy (defined as for figure 6) and (b) the signal/background ratio, both for the structure at near-normal incidence, as a function of incident-beam energy. The symbol diameters represent $\pm 1\ \sigma$ on the ordinate; the beam energies were stable to within $\sim$0.5 eV. The filled symbols relate to curve (b).

is clearly close to the maximum possible with this electron beam. The limiting case arises when any conceivable inelastic scattering event would reduce the electron energy below the threshold for core ionization, E_c. For silicon, this would be at an excess energy equal to the band gap, $\sim$1.2 eV ($\sim$1840 eV primary beam energy), although the most probable inelastic event is plasmon creation, requiring $\sim$17 eV: the bulk free-electron plasmon energy in Si is 16.6 eV [10], and the plasmon loss peaks occur at 17 ± 0.5 eV in both our XPS and electron-energy-loss data, in accord with results of previous workers [7, 10]. As the incident-beam energy E increases, scattered electrons must contribute increasingly to the core ionization which is the precursor of the detected x-ray emission, and if the angular spread of these electrons is greater than that of the incident beam, a reduction in anisotropy will result. The noticeable reduction in anisotropy which accompanies an increase in energy from 1849 to 1854 eV (figure 6) shows that electrons which have suffered losses much smaller than the plasmon energy E_p must contribute significantly to the process. Although plasmon creation is the most probable energy-loss process, electrons which have suffered lower-energy losses (by interband electronic excitations) will have a higher energy above the threshold and so will make a greater contribution to the x-ray yield. No step is seen at $E = E_c + E_p$ because at the threshold ($E = E_c$), the ionization cross-section is only about a quarter of that at $E = E_c + E_p$ (see figure 8), but the contribution from the scattered electrons following a plasmon-creation energy loss will increase progressively with increasing excess energy. Similar comments apply to the threshold for two-plasmon losses ($E = E_c + 2E_p$); again no step is discernible, either in the energy dependence of the anisotropy or in that of the total Si Kα yield, as reflected in the curve (b) in figure 8.

Two significantly different mechanisms could, however, contribute to the reduction in the anisotropy. If the inelastic scattering events are accompanied by only small changes in direction, then the effective angular resolution of the experiment will decline with increasing incident energy, and angular fine detail will be lost as the extent of anisotropy is reduced. At the same time, the effective sampling depth will be increased because, on average, the

electrons will have travelled further into the solid before inducing a core ionization. If, on the other hand, inelastic scattering events are accompanied by deflections that are large compared with the angular width of the diffraction features, then the x-ray flux derived from the scattered electrons will be effectively almost isotropic, contributing to the background but not to the signal. The anisotropy will decrease, but the signal quality will not be greatly impaired and would have a sampling depth governed by the inelastic mean free path appropriate to the incident energy. The recent literature is conflicting on this: Puppin *et al* [7] cite a formula due to Raether [37] suggesting that an 1850 eV electron beam would be deflected by no more than 0.26° after a single plasmon-creation event, while Erbudak *et al* [38] suggest, on the basis of experimental observations, that plasmon creation is associated with substantial directional changes, greater than those accompanying electronic excitations. Little change was observed in the XPD band profile in figure 6 over a 35 eV change in energy, and the overall profiles in figures 4 and 5 (with a 15 eV energy difference) are not noticeably different, suggesting that over this range at least, the signal degradation is not great. This observation is, however, compatible with either hypothesis. It is nevertheless clear from our preliminary studies on GaAs [18] that by 73 eV above the threshold, there is substantial loss of fine structure, indicating that scattering through small angles is important, and that consequently some signal degradation may reasonably be expected as the incident energy is increased.

There is, moreover, little practical advantage in increasing the incident-beam energy. The increase in the absolute level of the h/b signal is almost entirely offset by the reduction in anisotropy, so the data collection times required for similar signal/noise ratios in the iXPD pattern remain almost the same. However, working very close to the threshold for core ionization may introduce a risk of band-structure effects: if the ionized electron is not fully free, there may be some possibility of an angular dependence in the ionization probability, and the signal becomes inconveniently small relative to the background. Selecting an energy about 5–10 eV above the threshold should generally offer a good compromise for high-resolution iXPD studies.

We return now to the variation of the Si Kα peak height/background ratio (h/b) with incident-beam energy, shown in figure 8 (curve (b)). Data were also collected at 1904, 1944, 2046, 2240 and 2493 eV, yielding values of h/b of 6.5, 12, 34, 98 and 229: these are not shown in the figure to avoid obscuring the near-threshold behaviour. Between 1840 and 2500 eV, the intensity of the bremsstrahlung background should increase with energy by ∼37% [39]. The ratio between the parameter h/b and the calculated ionization cross-section should therefore decline slowly with increasing energy if the theoretical approach is adequate in this very-near-threshold regime. Using Gryzinski's simple equation for the cross-section for atoms [40], in which the ionization function g_i depends solely on the ratio between the kinetic energy of the incident electron and the binding energy of the core electron, denoted as x:

$$g_i(x) = \frac{1}{x}\left(\frac{x-1}{x+1}\right)^{3/2}\left\{1+\frac{2}{3}\left(1-\frac{1}{2x}\right)\ln\left[2.7+(x-1)^{1/2}\right]\right\}$$

this ratio in fact passes through a minimum at ∼1950 eV (110 eV above the threshold), *increasing* roughly linearly by ∼78% by 2500 eV. Below 1950 eV, the ratio increases increasingly rapidly, exceeding the 2500 eV value below 1859 eV and tending to infinity at the threshold: Gryzinski's formula predicts a vanishing cross-section at the threshold, while the data indicate a relatively small but finite value. However, if the core binding energy is replaced in the equation by a value only 13 eV lower (i.e. 1826 eV rather than 1839 eV), the form of the variation in h/b over the region 0–50 eV above the threshold is reproduced

to within 1.5%. (Gryzinski did in fact note that the use of the orbital binding energy here constituted a 'rough assumption'.) The steady increase in (h/b)/cross-section over the next 600 eV remains virtually unchanged by this modification, but this increase is likely to be due to the increase in sampling depth as the contribution to the x-ray yield from inelastically scattered electrons increases. With minor modifications, Gryzinski's atomic approach thus adequately accounts for the present limited data.

Finally, we consider how the sensitivity of iXPD is likely to vary from one substrate to another, and whether it can be improved experimentally. The ionization cross-section for any core level is proportional to (ionization energy)$^{-2}$ [40], suggesting that the sensitivity of the iXPD procedure could be ∼4 times greater at ∼900 eV. However, the alternative core-hole decay route via Auger electron emission becomes much more probable at low atomic number [41], offsetting the gain in cross-section. The balance between these factors will vary from case to case, but there seems no reason to expect a great improvement for systems with either greater or lesser core binding energies. However, the width of the major XPD features generally *decreases* as the electron energy increases [31], so it would be worthwhile to explore the practicality of iXPD measurements at higher energies. Studies of compound substrates will also be more difficult than those of elemental solids, since all of the elements present will contribute to the background but not to the desired signal.

On the experimental side, current Si(Li) detector systems operate very close to the fundamental limits for energy resolution [42], so there is little scope for improving the ratio h/b by improving the energy resolution within this technology. Wavelength-dispersive x-ray analysis offers much higher resolution, but x-ray collection would then be over such a small solid angle that the sensitivity overall would be unlikely to be improved. Because the limitation on data collection time is set by the rate at which the Si(Li) x-ray detection system can operate, increasing the incident-beam current further does not assist in improving the sensitivity. Moving the detector closer to the sample is feasible, but would only permit a reduction in beam current, not a reduction in data collection time, and might result in increased sample contamination rates. At the present time, therefore, developments in the pulse processing technology [42] to permit higher data acquisition rates would seem to offer the best hope for improvement.

5. Conclusions

The feasibility of a reversal of the conventional XPD experiment, in which the probability of incident electrons being diffracted to reach specified sites is monitored by characteristic x-ray emission from those sites, subsequent to core ionization induced by the incident beam, has been demonstrated using Si(100), rotated about a ⟨110⟩ axis to generate variable-polar-angle diffraction data. The expected close parallels with XPD have been established, and the new technique, termed 'inverted' XPD, has provided higher angular resolution than previous studies of this substrate. The forward-scattering maxima associated with the high-atomic-density directions [001], [114], [112] and [111] have been shown to exhibit previously undetected splittings similar to those explained by analogy with Kikuchi-band theory (and also recently observed in high-resolution XPD at normal electron exit from Si (111) [13]). However, with currently available technology, the collection of data with good statistics is slow, and even in ultra-high vacuum sample contamination is a problem. If, however, the x-rays could be detected using much higher energy resolution but over the same (or a greater) solid angle, the signal/background ratio would be greatly increased, and the utility of the new technique greatly expanded.

Acknowledgment

The EPSRC (formerly the SERC) is thanked for support under Standard Grant GR/H 26864.

References

[1] Fadley C S 1990 *Synchrotron Radiation Research: Advances in Surface Science* ed R Z Bachrach (New York: Plenum)
[2] Grenet G, Jugnet Y, Poon H C and Duc Tran Minh 1989 *Surf. Interface Anal.* **14** 367
[3] Osterwalder J, Aebi P, Fasel R, Naumovic D, Schwaller P, Kreutz T, Schlapbach L, Abukawa T and Kono S 1995 *Surf. Sci.* **331–333** 1002
[4] Hill J M, Royce D G, Fadley C S and Wagner L F 1976 *Chem. Phys. Lett.* **44** 225
[5] Kubler L, Lutz F, Bischoff J L and Bolmont D 1991 *Surf. Sci.* **251+252** 305
[6] Kubler L, Lutz F, Bischoff J L and Bolmont D 1992 *Surf. Interface Anal.* **19** 336
[7] Puppin E, Carbone C and Rochow R 1992 *Phys. Rev.* B **46** 13 215
[8] Tonner B P, Zhang J, Chen X, Han Z-L, Harp G R and Saldin D K 1992 *J. Vac. Sci. Technol.* B **10** 2082
[9] Bischoff J L, Kubler L, Lutz F, Diani M and Bolmont D 1992 *Solid State Commun.* **83** 823
[10] O'Brien W L, Zhang J and Tonner B P 1993 *Phys. Rev.* B **48** 10 934
[11] Fraxedas J, Ferrer S and Comin F 1994 *Surf. Sci.* **307–309** 775
[12] Pirri C, Kafader U, Gewinner G and Wetzel P 1994 *Solid State Commun.* **89** 313
[13] Gewinner G, Kafader U, Wetzel P and Pirri C 1994 *J. Electron Spectrosc. Relat. Phenom.* **67** 387
[14] Bullock E L, Gunnella R, Patthey L, Abukawa T, Kono S, Natoli C R and Johansson L S O 1995 *Phys. Rev. Lett.* **74** 2756
[15] White R C, Fadley C S and Trehan R 1986 *J. Electron Spectrosc. Relat. Phenom.* **41** 95
[16] Osterwalder J, Stewart E A, Cyr D, Fadley C S, Mustre de Leon J and Rehr J J 1987 *Phys. Rev.* B **35** 9859
[17] Egelhoff W F 1987 *Phys. Rev. Lett.* **59** 559
[18] Evans S 1995 *J. Electron Spectrosc. Relat. Phenom.* **70** 217
[19] Pendry J B 1981 *J. Phys. C: Solid State Phys.* **14** 1381
[20] See, for example,
See A K, Thayer M and Bartynski R A 1993 *Phys. Rev.* B **47** 13 722
[21] Evans S and Riley C E 1986 *J. Chem. Soc. Faraday Trans.* II **82** 541
[22] Anthony M T and Seah M P 1984 *Surf. Interface Anal.* **6** 95
[23] Taylor J A 1981 *Appl. Surf. Sci.* **7** 168
[24] Evans S and Hiorns A G 1986 *Surf. Interface Anal.* **8** 71
[25] Goldstein J I, Newbury D E, Echlin P, Joy D C, Fiori C and Lifshin E 1981 *Scanning Electron Microscopy and X-ray Microanalysis* (New York: Plenum) pp 396–401
[26] Evans S 1992 *Surf. Interface Anal.* **18** 323
[27] Flitsch R and Raider S I 1975 *J. Vac. Sci. Technol.* **12** 305
[28] Xu M-L and Van Hove M A 1989 *Surf. Sci.* **207** 215
[29] Sipr O 1991 *J. Phys.: Condens. Matter* **3** 8503
[30] Egelhoff W F 1984 *Phys. Rev.* B **30** 1052
[31] Goldberg S M, Baird R J, Kono S, Hall N F T and Fadley C S 1980 *J. Electron Spectrosc. Relat. Phenom.* **21** 1
[32] Chambers S A and Tran T T 1994 *Surf. Sci.* **314** L867
[33] Agliz D, Quémerais A and Sébilleau D 1995 *Surf. Sci.* **343** 80
[34] Varma S, Chen X, Davoli I, Saldin D K and Tonner B P 1994 *Surf. Sci.* **314** 145
[35] Parry D E 1996 private communication
[36] Wagner C D 1983 *Practical Surface Analysis by Auger and X-ray Photoelectron Spectroscopy* ed D Briggs and M P Seah (Chichester: Wiley) p 488
[37] Raether H 1980 *Excitation of Plasmons and Interband Transitions by Electrons (Springer Tracts in Modern Physics 88)* ed G Holer (New York: Springer)
[38] Erbudak M, Hochstrasser M and Wetli E 1994 *Phys. Rev.* B **50** 12 973
[39] Tertian R and Claisse F 1982 *Principles of Quantitative X-ray Fluorescence Analysis* (London: Heyden) p 40
[40] Gryzinski M 1965 *Phys. Rev.* **138** A336
[41] Hagedoorn H L and Wapstra A H 1960 *Nucl. Phys.* **15** 146
[42] Gedcke D A 1974 *Quantitative Scanning Electron Microscopy* ed D B Holt, M D Muir, P R Grant and I M Boswarva (London: Academic) p 422